Microporous and Mesoporous Materials 267 (2018) 212–220

Contents lists available at ScienceDirect

Microporous and Mesoporous Materials

journal homepage: www.elsevier.com/locate/micromeso

Zeolitic imidazole Framework-8 (ZIF-8) fibers by gas-phase conversion of electroblown zinc oxide and aluminum doped zinc oxide fibers

Jani Holopainen[a,*], Mikko J. Heikkilä[a], Leo D. Salmi[a,1], Kaisu Ainassaari[b], Mikko Ritala[a]

[a] Department of Chemistry, University of Helsinki, P.O. Box 55, FI-00014, University of Helsinki, Finland
[b] Environmental and Chemical Engineering, Faculty of Technology, University of Oulu, P.O. Box 4300, FI-90014, University of Oulu, Finland

ARTICLE INFO

Keywords:
Electroblowing
Nanofibers
Zinc oxide
Metal organic frameworks
Gas-phase conversion

ABSTRACT

Electroblowing was used to prepare ZnO and aluminum doped zinc oxide (AZO, 1–3 cation-% of Al) fibers. The as-blown fibers were calcined at 500 °C to obtain the target material. The average fiber diameters ranged from 240 ± 60 nm for ZnO fibers to 330 ± 80 nm for AZO with 3% Al. Smaller crystallite size was measured with x-ray diffraction for the Al doped fibers. Electroblowing was found out be an effective method to increase the fiber productivity over electrospinning and other methods reported in literature to prepare AZO fibers as a high production rate of 0.32 g/h was achieved. The ZnO and AZO fibers could be converted to zeolitic imidazole framework-8 [ZIF-8, zinc(2-methylimidazolate)$_2$] by a solvent free thermal treatment in an autoclave under 2-methylimidazole (HmIM) vapor at 150 and 200 °C while preserving the fibrous structure. The conversion process to ZIF-8 occurred faster at higher temperatures and on fibers with smaller crystallite size. Depending on the conversion treatment time either ZnO/ZIF-8 and AZO/ZIF-8 core/shell fibers or ZIF-8 fibers could be obtained. At best the prepared ZIF-8 fibers had a very high BET specific surface area of 1340 m^2/g.

1. Introduction

Metal organic frameworks (MOFs) are hybrid materials consisting of metal ions or clusters connected by organic linker molecules. Owing to their inherent nanoporous network structure, MOFs have applications in areas such as gas sensing, gas storage and catalysis [1,2]. Recently they have been studied also for a wide variety of electronic and optoelectronic applications in the form of patterned structures, which has sparked demand for new conformal synthesis methods down to the nanoscale [3,4]. Nanofibers as interconnected fibrous networks have great interest for such applications where a large and readily accessible surface area is required. For example, porous nanofibers with large surface to volume ratio combined with high specific surface area are promising as energy storage materials for lithium ion batteries and supercapacitors [5].

Zeolite imidazole framework-8 (ZIF-8, zinc(2-methylimidazolate)$_2$) is a MOF material that comprises of tetrahedrally coordinated zinc ions connected by 2-methylimidazolate linkers in a zeolite-like topology [6]. Most commonly ZIF-8 is prepared via solvothermal synthesis methods, but preparing patterned structures through these routes is difficult [4,7]. Recently a new method for ZIF-8 synthesis has emerged that relies on the conversion of ZnO to ZIF-8 via a reaction between solid ZnO and 2-methylimidazole (HmIM) vapor [8,9]. This gas phase conversion enables the preparation of conformal ZIF-8 coatings with a uniform thickness, controlled at a much more accurate level compared to the more commonly used solvothermal preparation methods. Thus far this gas phase conversion of ZnO to ZIF-8 has been restricted to thin films.

To the authors' knowledge there are no reports on preparation of ZIF-8 fibers, nor any other MOF material in the bare fiber form, but ZIF-8 has been incorporated as particles within fiber matrices and as a coating on fibers. Electrospinning is the most well-known and most used method to prepare long continuous polymer nanofibers and, via calcination of polymer fibers containing additional precursors, also ceramic fibers [10–12]. Composites consisting of polymer fibers loaded with ZIF-8 particles have also been prepared by electrospinning [13–15]. An atomic layer deposited ZnO thin film on electrospun polyacrylonitrile fibers has been solvothermally converted to a ZIF-8 coating [16]. Tellurium nanowires [17] and polymer fibers [18,19] have been directly coated with ZIF-8 by crystallization of ZIF-8 from a solution onto the fiber surfaces. Similarly TiO_2 nanofibers have been coated with ZIF-8 by sonochemical crystallization from a ZIF-8 precursor solution [20], and recently also ZnO nanowires and electrospun ZnO fibers have been solvothermally coated with ZIF-8 for gas sensing applications [21,22].

* Corresponding author.
E-mail address: jani.holopainen@helsinki.fi (J. Holopainen).
[1] Present Addresses. ASM Microchemistry, Pietari Kalmin katu 1 F 2, FI-00560 Helsinki, Finland.

https://doi.org/10.1016/j.micromeso.2018.04.003
Received 21 February 2018; Received in revised form 23 March 2018; Accepted 1 April 2018
Available online 03 April 2018

ZnO in itself is an interesting semiconductor material with optical and electrical properties that can be tuned for various applications by doping with different elements. For example Al or Ga doped ZnO provides a cheaper and less toxic alternative to the commonly used indium tin oxide (ITO) transparent thin film electrodes for solar cells [23–26]. ZnO and doped ZnO fibers are especially interesting for gas sensing and optoelectronic applications due to their high surface to volume ratio. There are several reports in the literature on electrospinning of ZnO, doped ZnO and various metal oxide/zinc oxide composites [27–45]. Al doping has been used to improve the conductivity of ZnO [41–45]. Fibers of bare ZnO [29,30], ZnO doped with cobalt [31], copper [32], cerium [33] and cadminum [34], and ZnO/SnO2 [35,36] and ZnO/In_2O_3 [37] composites have been used as gas sensors. ZnO/SnO_2 [38,39] and ZnO/NiO [40] have been studied as high capacity anodes for lithium ion batteries.

Although the excellent controllability of fiber properties and the wide range of attainable materials have made electrospinning the most popular nanofiber preparation method, its industrial applicability is limited due to its modest production rate [46]. Conventionally fibers have been spun from a single needle in which case typical solution flow rates are in the range of 0.1–2 ml/h and fiber productivity around 0.1 g/h and even less in the case of ceramic fibers. Upscaling via multiplication of needles is complicated because the electric fields at the needle tips are altered by the nearby needles significantly affecting the spinning process [47]. Needleless designs relying on self-formation of Taylor cones on polymer solution surfaces have shown improved upscalability, but typically have somewhat less control on the fiber properties [48–52].

Solution blow spinning has recently emerged as a new straightforward method for improving fiber productivity [53–55]. It relies on a high velocity gas flow to draw a polymer solution into fibers. The method has gained significant interest especially in the preparation of nanofibers for biomedical applications. As compared to the needle electrospinning substantially higher solution feed rates can be used and thus productivity is significantly increased. Electroblowing is a combined method of both the conventional needle electrospinning and solution blow spinning, i.e. both high voltage and high velocity gas flow are used to form fibers from a solution [56–58]. The main jet drawing force is the high velocity gas flow and thus high production rates comparable to solution blow spinning can be obtained. Similarly to electrospinning the repulsion between the charges in the polymer jets in electroblowing results in a randomly oriented fiber network with less bundling of fibers as compared to the solution blow spinning [59,60].

Significantly less materials have been prepared by solution blow spinning and electroblowing as compared to electrospinning. Especially reports on preparation of inorganic fibers are scarce. Solution blow spinning has been used to prepare ZnO [61] and via pyrolysis of solution blown zinc acetate/polyacrylonitrile also ZnO encapsulated carbon [62] nanofibers. Alumina fibers have also been solution blow spun and electroblown, though only with relatively large average fiber diameters of 4.12 and 2.75 μm, respectively [58].

In this study we used electroblowing to prepare ZnO and conductive aluminum doped zinc oxide (AZO) nanofibers. To the authors' knowledge there are no prior reports on electroblowing of these materials in the literature. Further on we used the prepared fibers as templates for the preparation of ZIF-8 fibers. The ZnO and AZO fibers were converted to ZIF-8 by thermal treatment under HmIM vapor in an autoclave at 150 and 200 °C. Depending of the conversion parameters core/shell or bare ZIF-8 fibers were obtained. This is to the best of our knowledge also the first report on the preparation of bare ZIF-8 or any other kind of metal-organic framework fibers.

2. Experimental

The electroblowing solutions were prepared by dissolving of Zn$(NO_3)_2{\cdot}4H_2O$ (Merck, 98.5%) and Al$(NO_3)_3{\cdot}9H_2O$ (J.T. Baker, 98.6%) in appropriate amounts of deionized water followed by addition of DMF (Sigma-Aldrich, 99.9%) and a beforehand prepared 18 wt % PVP (Aldrich, M_w = 1 300 000) in EtOH (VWR Chemicals, 96%) solution (Table 1). The aluminum content varied from 0 to 3 mol. % in respect to the Zn and Al in the solution [Al/(Al + Zn)]. Additionally some experiments were performed on electroblowing of ZnO with solutions where either H_2O or DMF was fully replaced with the other one in the solvent (Supporting information, Table S1).

Table 1
The electroblowing solutions.

Solution	Zn$(NO_3)_2{\cdot}4H_2O$ (g)	Al$(NO_3)_3{\cdot}9H_2O$ (g)	H_2O (ml)	DMF (ml)	18 wt % PVP/EtOH (ml)
ZnO	1.0	–	2	4.5	7.5
AZO-1	1.0	0.014	2	4.5	7.5
AZO-2	1.0	0.029	2	4.5	7.5
AZO-3	1.0	0.044	2	4.5	7.5

A self-made apparatus was used to blow the solutions into fibers. Compressed air was delivered through a custom made 3 mm metal nozzle at a rate of 30 Nl/min. A 27G needle was pushed through the nozzle and placed at the center of the gas flow protruding ~2 mm from the aperture. The needle was connected to a 10 ml syringe and the solution was pushed through the needle at rate of 15 ml/h with a syringe pump (KDS Legato™). The needle and nozzle were set to 15 kV with a high voltage power source. The solution jet ejected from the needle tip was collected as fibers on grounded metal grid collectors. A cylindrical collector with a diameter of 50 cm and a planar back collector 80 cm from the nozzle were used similarly to our previous study [63]. The collectors were enclosed in a box with an additional drying gas flow (40 Nl/min) for efficient solvent vapor removal from the box through the holes located behind the back collector. The relative humidity within the box during the experiments remained below 15%. The as-blown fibers were calcined to the target material in an ashing furnace at 500 °C in air for 4 h, unless otherwise noted in the text. Some ZnO samples were calcined at 400 and 600 °C for 4 h. When necessary for comparative purposes the calcination temperatures used to prepare the ZnO fibers are indicated as ZnO@400 °C, ZnO@500 °C and ZnO@600 °C. Regardless of the calcination temperature a heating rate of 1 °C/min was always used.

The ZnO and AZO fibers were converted to zeolitic imidazole framework-8 (ZIF-8) by thermal treatment in 2-methylimidazole (HmIM) vapor in an autoclave (Parr 4744). First 0.5 g of HmIM was placed at the bottom of the autoclave. Next approximately 0.05 g of fibers were placed inside a glass vial that was inserted in the autoclave. The autoclave was closed and placed in an oven at 150 °C or 200 °C for variable time periods. After the treatment the autoclave was let to cool and the fibers were removed and placed in an oven at 150 °C for at least 2 h to remove any residual HmIM from the samples.

The prepared fibers were imaged with scanning electron microscopy (SEM) and scanning transmission electron microscopy (STEM) in a Hitachi S-4800 field emission SEM. Prior to SEM characterization 4 nm of Au/Pd was sputtered onto the fibers to enhance image quality. Image J software was used to determine the average fiber diameters from measurements of 100 individual fibers in each sample. The crystal structures were analyzed with a PANalytical X'Pert Pro MPD X-ray diffractometer using CuKα-radiation. The crystallinity and phase compositions were analyzed with a PANalytical X'Pert Pro MPD X-ray diffractometer using CuKα-radiation and parallel beam optics. The apparent crystallite sizes and the ZIF-8 to ZnO phase ratios were determined from the XRD data by Rietveld refinement using the MAUD software [64,65]. Thermogravimetric analyses (TGA) were conducted with a Mettler Toledo Star^e system equipped with a TGA 850 thermobalance using a heating rate of 10 °C/min between 25 and 800 °C in air and N_2. The BET specific surface areas and pore size distributions were

determined by N_2 physisorption measurements at 77 K (Micromeritics ASAP 2020). The p/p_0 range used for the BET calculation was 0.05–0.25.

For the electrical measurements approximately 1×3 cm^2 fiber sheets were cut from the calcined fiber sheets and placed on non-conductive glass substrates. Silver paste was used to make contacts on the full length of the 1 cm edges and the resistance of the fiber sheet over the 3 cm length was measured with a digital multimeter. The measurements were only used to qualitatively determine the effect of Al content on the conductivity of the fibers.

3. Results

The electroblowing of ZnO nanofibers was done using poly(vinyl pyrrolidone) (PVP) as the carrier polymer and zinc nitrate as the zinc source that were selected based on initial screening tests. The same zinc precursor/polymer combination has been used in electrospinning by Mali et al. [27] albeit with just water and ethanol (EtOH) as the solvents, and by Zhao et al. [38] with N,N-dimethylformamide (DMF) and EtOH as solvents. In literature electrospinning of ZnO has been performed also using various other zinc precursors and carrier polymers.

Due to the increased feed rate of the solution, electroblowing is somewhat more sensitive to the solution properties compared to the conventional single needle electrospinning. A solvent combination of 2 ml of water, 4.5 ml of DMF and 7.5 ml of 18 wt % PVP/EtOH solution was used to optimize the electroblowing of $Zn(NO_3)_2$/PVP and Al $(NO_3)_3$/$Zn(NO_3)_2$/PVP composite fibers. It was found out to yield a stable electroblowing process and to produce good quality nanofibers. In contrast, we were unable to make a solution consisting of just EtOH and water that would have resulted in a stable ZnO electroblowing process, while simply using a combination of DMF and EtOH produced fibers with slightly larger diameters than the H_2O/DMF/EtOH combination (Supporting information, Fig. 1 and Table S1).

After calcination of the as-spun composite fibers at 500 °C, the obtained ZnO and AZO (1–3 cation-% Al) fibers were continuous and had a random orientation as seen by scanning electron microscope (SEM) (Fig. 1). After calcination the ZnO fibers had a diameter of 240 ± 60 nm while doping with aluminum resulted in a slight increase in the fiber diameter within the tested range of 0–3% Al (Table 2). The fiber diameter increased from the 240 ± 60 nm for the ZnO fibers to 330 ± 80 nm for the AZO fibers with 3% Al.

Table 2
Fiber diameters and crystallite sizes of ZnO and AZO fibers. All results are from the fibers calcined at 500 °C for 4 h. The crystallite sizes were calculated from the XRD data in Fig. 2.

Sample	Fiber diameter[a]	Apparent crystallite size
ZnO	240 ± 60 nm	128 nm
AZO-1	280 ± 80 nm	41 nm
AZO-2	280 ± 70 nm	25 nm
AZO-3	330 ± 80 nm	19 nm

[a] Mean ± standard deviation.

Already in SEM it was clearly seen that the AZO fibers had a smaller crystal size compared to the ZnO fibers and as a consequence the AZO fibers with higher aluminum contents were also smoother (Fig. 2). Likely due to the decrease in crystallite size the aluminum doped fiber sheets were also less fragile and could be bent somewhat before fracturing whereas the ZnO fiber sheets were very rigid and fragile. However, no quantitative analyses on the mechanical properties were performed.

In the x-ray diffraction (XRD) on the ZnO and AZO fibers the characteristic reflections of hexagonal ZnO (zincite) were observed with no additional reflections regardless of the Al content (Fig. 3). Due to the smaller crystal size the observed reflections were broader for the fibers with the higher aluminum contents. The apparent crystallite size decreased from 128 nm for ZnO to 19 nm for AZO-3 (Table 2). The crystallite size in AZO and ZnO fibers was also strongly dependent on calcination temperature. The crystallite size of ZnO could be decreased to 33 nm by reducing the calcination temperature to 400 °C (ZnO@400 °C fibers) and also increased by a higher calcination temperature (Supporting information, Fig. S2). Thus modifying the calcination

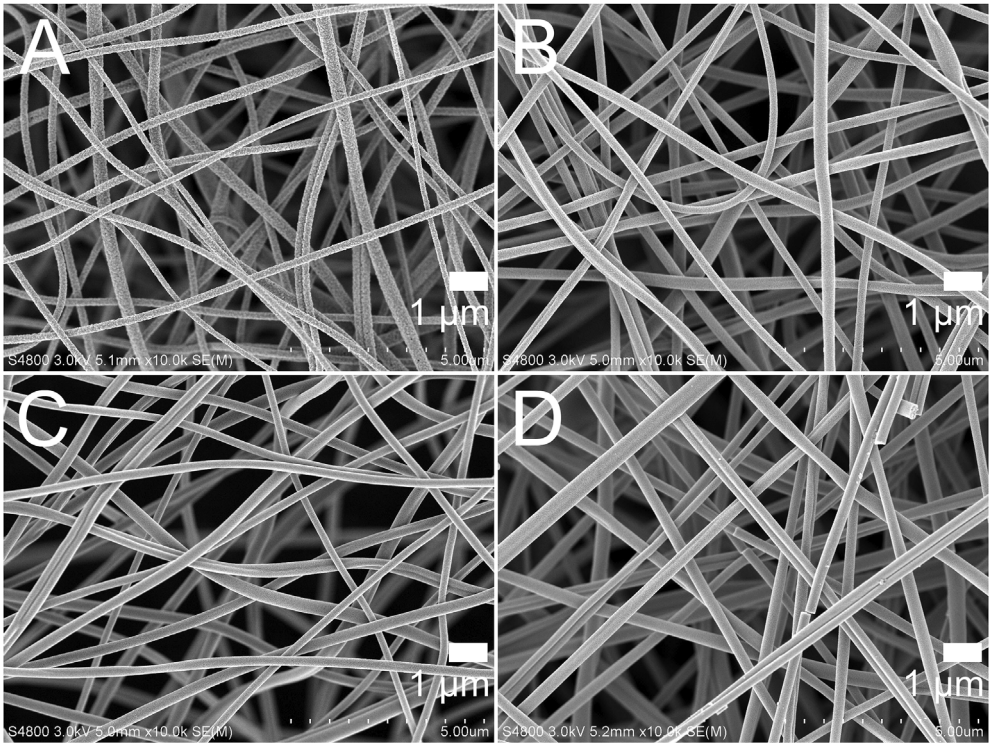

Fig. 1. SEM images of (A) ZnO fibers, and AZO fibers with (B) 1, (C) 2 and (D) 3% Al.

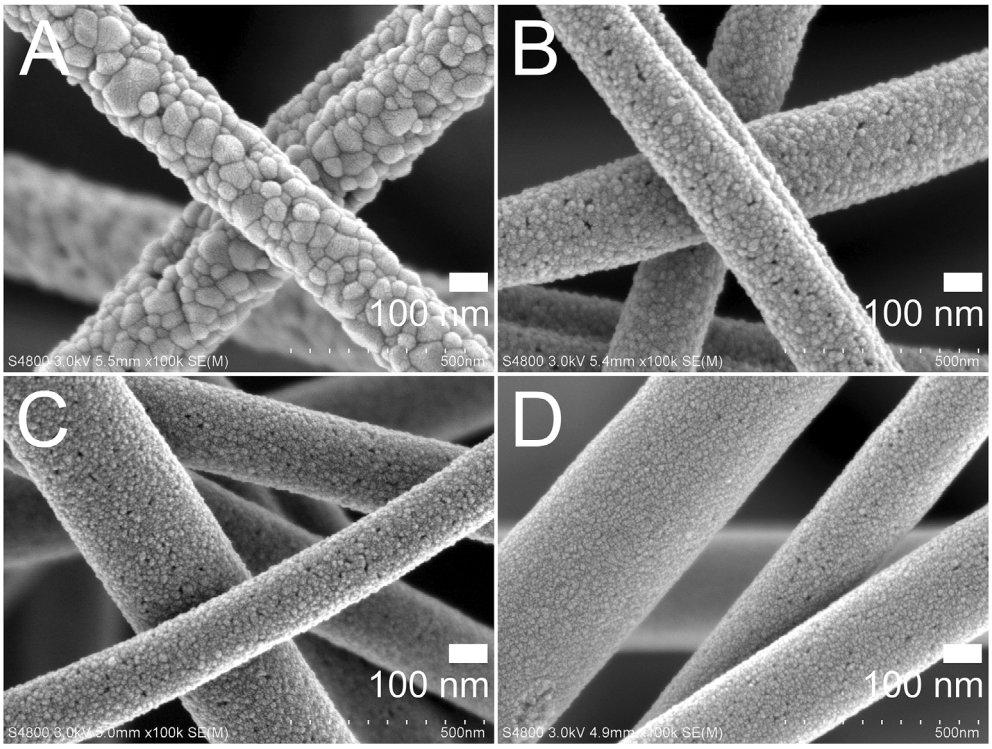

Fig. 2. High magnification SEM images showing the surface topography of (A) ZnO fibers, and AZO fibers with (B) 1, (C) 2 and (D) 3% Al.

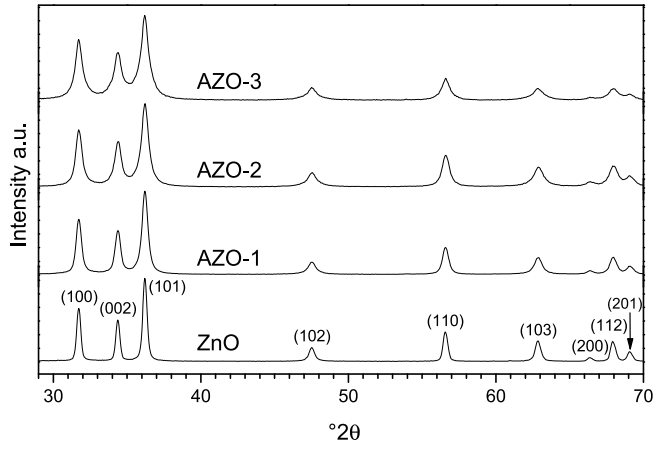

Fig. 3. XRD of AZO fibers with 0–3% Al. All the observed reflections were assigned to the zincite phase. The intensities in the diffractograms have been normalized in respect to the highest peak intensity in each.

temperature offers a straightforward way to optimize the crystallite size e.g. for gas sensor applications.

Relatively high solution feed rates can be used in electroblowing, which enables the preparation of nanofibers at a very high rate compared other nanofiber spinning methods. The measured fiber production rates were 0.31 g/h for ZnO and 0.32 g/h for AZO fibers when using a solution feed rate of 15 ml/h. In comparison, the feed rates reported in electrospinning studies on ZnO and AZO fibers are typically ≤1 ml/h. Costa et al. used feed rates of 4.4 and 10 ml/h in solution blow spinning of ZnO fibers with PVP and poly(vinyl chloride) as the carrier polymers, respectively [61]. Thus by using electroblowing, substantially higher feed rates could be used in this study and consequently the production rate is greatly improved from the conventional electrospinning and also somewhat from the solution blow spinning. Compared to the solution blow spun fibers the electroblown fibers are also less bundled. A recent study found electroblowing to result in thinner fibers and more homogeneous fiber diameter distribution compared to solution blow spinning [58]. In our previous study on the preparation of hydroxyapatite fibers, we showed electroblowing to result in superior fiber quality as compared to solution blow spinning [63].

The conductive properties of the prepared fibers were evaluated qualitatively by measuring the resistance of the calcined AZO fiber sheets with a width of 1 cm over a length of 3 cm (Supporting information, Fig. S3). It should be noted that as the porosity and thickness of the individual sheets could not be determined accurately enough, the results cannot be used for quantitative analysis of the electrical properties. Anyhow, as the sheets were always cut from the center of the back collector for all samples and the differences between the electroblowing solutions were minor, the differences in porosities and sheet thicknesses should be small between the different samples and thus the measurements could be used for a rough comparison of the samples. Based on the measured resistances the highest conductivities were obtained with 1 and 2% Al whereas with 3% the resistance was higher and bare ZnO fibers could not be measured. Comparable results have been reported in the literature where Cho and Kuo obtained the lowest resistivity values for AZO fibers with 2% Al followed by an increase of resistivity with higher Al content [45]. Similarly Lotus et al. reported AZO fibers with 1.7% Al to have the highest conductivity when compared to fibers with 0, 2.4 and 3.2% Al [42].

ZIF-8 fibers were prepared from the ZnO and AZO-3 fibers by thermal conversion in an autoclave under HmIM vapor at 150 °C and 200 °C for 18, 42 and 68 h. Regardless of the temperature and starting material a continuous ZIF-8 layer had formed on the fibers after 18 h (Fig. 3 and Supporting information Figs. S4 and S5) and significant thickening of the fibers was observed compared to the bare ZnO and AZO-3 fibers. SEM imaging indicated that upon prolonged vapor exposure more rapid thickening was occurring in the conversion of the AZO-3 and ZnO@400 °C fibers compared to the ZnO@500 °C fibers. After 18 h the average fiber diameters were 470 ± 120 and 600 ± 120 nm for the ZIF-8 fibers converted at 150 °C from ZnO and AZO-3, respectively (Supporting information Fig. S4). This means an

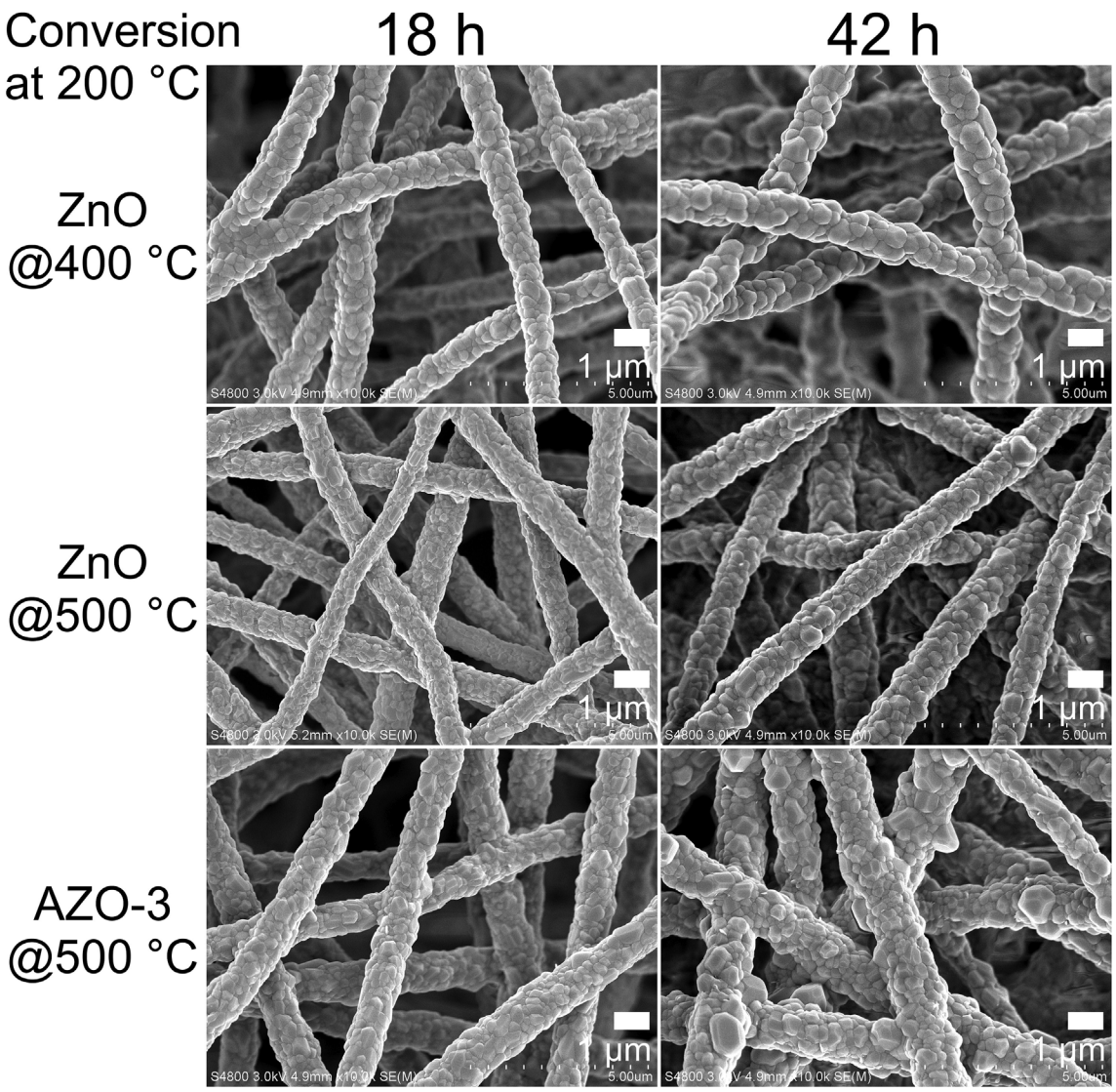

Fig. 4. SEM images of ZIF-8 fibers prepared from ZnO calcined at 400 °C (upper row) and 500 °C (center), and AZO-3 (bottom) by the conversion treatment at 200 °C for (left) 18 h and (right) 42 h.

increase of 230 nm from the ZnO and 270 nm from the AZO-3 fibers used as the starting materials. ZnO fibers prepared by calcination at 400 °C (ZnO@400 °C) and subjected to the vapor conversion (Supporting information, Fig. S5) were 560 ± 120 nm in diameter after 18 h. The diameters of the fibers converted at 200 °C (Fig. 4) were much larger than those of the fibers converted at 150 °C as after 18 h at 200 °C the fiber diameters were already 1010 ± 180, 970 ± 190 and 1150 ± 190 nm for ZnO@400 °C, ZnO@500 °C and AZO-3, respectively.

In addition to the increase in diameter, from SEM images it also appeared that the ZIF-8 crystallites were growing in size upon increase in treatment time (Supporting information, Fig. S6). A similar coalescence of ZIF-8 crystals was reported by Kwon et al. when subjecting ZIF-8 crystals to HmIM vapor under comparable conditions [66].

The formation of crystalline ZIF-8 was verified by XRD where the ZIF-8 phase [Crystallography Open Database (COD) ID:7111971] was clearly detected in all the 18, 42 and 68 h thermal vapor converted samples whereas the reflections originating from the crystalline ZnO phase were gradually declining as a function of the conversion time at both 150 °C (Fig. 5) and 200 °C (Supporting information, Fig. S7). When starting from AZO-3 and ZnO@400 °C no signs of the zincite phase were present in XRD after 42 h of vapor exposure at 200 °C. For ZnO@500 °C indications of minor presence of ZnO was still observed after 42 h of treatment at 200 °C, but a full conversion to ZIF-8 was likewise achieved after 68 h. In contrast, all the fibers converted at 150 °C still had zincite reflections present after 68 h of vapor exposure, though in the case of AZO-3 the peaks were only barely visible.

Similar to the SEM imaging and XRD measurements, quantitative calculations of the ZIF-8 to ZnO ratios from the XRD measurements verified that the conversion was proceeding significantly faster at 200 °C than 150 °C (Fig. 6). Also the fibers with lower initial crystallinity were faster converted, i.e. the ZnO@400 °C with a crystallite size of 33 nm showed more rapid transformation to ZIF-8 compared to the 500 °C calcined ZnO fibers (crystallite size of 128 nm), but slower than that occurring with the 500 °C calcined AZO-3 fibers (crystallite size of 19 nm).

TGA measurements on bare ZIF-8 fibers, i.e. ZnO fibers converted under HmIM vapor at 200 °C for 68 h, showed that the prepared ZIF-8 phase is thermally stable to over 325 and 425 °C in air and N_2, respectively (Supporting information, Fig. S8). During annealing in air the ZIF-8 should decompose and react with the O_2 in air to form ZnO. Based on the molar masses of each compound this reaction should theoretically result in a weight residue of 35.8%. This closely matches the measured the residue of 35.3% measured with TGA after heating to

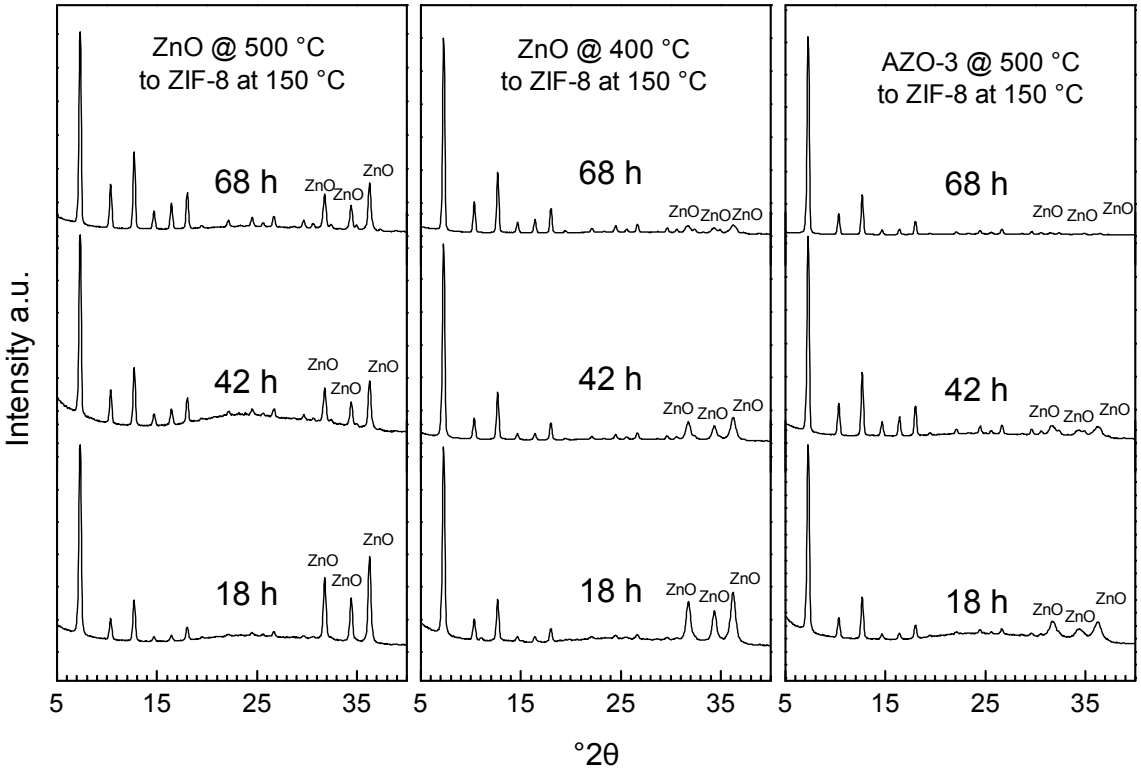

Fig. 5. XRD of fibers prepared by subjecting ZnO fibers calcined at 400 °C and 500 °C, and AZO-3 fibers to the HmIM vapor treatment at 150 °C in an autoclave for 18, 42 and 68 h. All the peaks were attributed to either ZnO or ZIF-8, and the ZnO peaks are marked separately. The intensities of the diffractograms have been normalized in respect to the highest peak in each pattern for better comparison on the progress of the ZnO to ZIF-8 transformation.

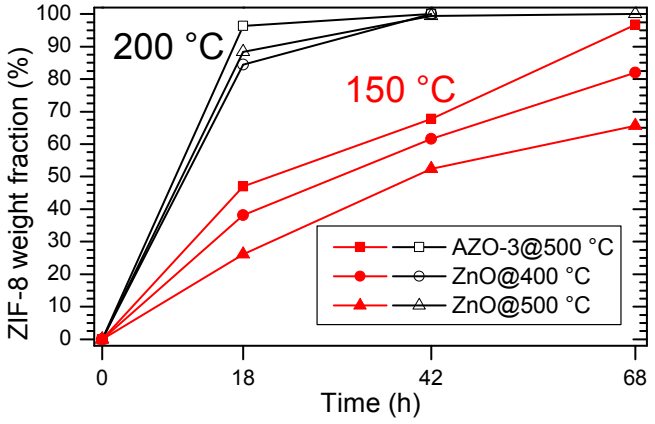

Fig. 6. The progression of the conversion of ZnO calcined at (▲) 400 °C and (■) 500 °C, and (●) AZO-3 to ZIF-8 at (red, closed symbols) 150 °C and (black, open symbols) 200 °C as a function of vapor treatment time. The ZIF-8 content was acquired from the Rietveld refinement of the XRD data. (For interpretation of the references to colour in this figure legend, the reader is referred to the Web version of this article.)

800 °C, suggesting that the prepared ZIF-8 is of high purity.

Our studies showed that during the conversion reaction the original fibrous structure was preserved and ZIF-8 formation was seen all along the fibers already at 150 °C, but the process was faster at 200 °C. However, the treatment temperature also had a noticeable effect on fiber homogeneity: despite the faster conversion the fibers converted at 200 °C were more homogenous in fiber diameter compared to the fibers converted at 150 °C to similar ZIF-8 fractions. Apparently the higher temperature promoted the initial nucleation of ZIF-8 resulting in a higher nucleation density and consequently more homogenous ZIF-8 crystal growth all along the fibers. In fact, in the conversion at 200 °C only 1–2 h of conversion was sufficient for the formation of a thin but smooth and continuous ZIF-8 layer around the ZnO fiber core, evident in both SEM and STEM (Fig. 7). However, it should be noted that due to the apparently weak crystallinity and small thickness of the formed layer, no ZIF-8 phase could be detected in XRD from the 1 h converted sample whereas in the 2 h converted sample the crystalline phase was clearly present (Supporting information, Fig. S9). In literature, Yanfeng et al. used a similar solvent-free conversion method to transform a ZnO film conformally into ZIF-8 in an autoclave at 180 °C [8]. Solvothermal treatment of electrospun ZnO in a solution of HmIM in DMF at 70 °C has been similarly reported to result in a continuous ZIF-8 coating all around the ZnO fiber core [22]. However, the solvothermal growth proceeded via formation of somewhat large crystallites on the ZnO fibers and 6 h of treatment was needed for the large crystals to merge into a continuous ZIF-8 coating. Consequently individual fibers had large diameter variations and were significantly rougher compared to the fibers prepared here via the gas phase conversion method.

STEM imaging verified that the conversion process occurs from the fiber surfaces towards the core of the fibers regardless of the conversion time. As seen from the STEM images of ZnO fibers converted at 150 and 200 °C for 18 h, a ZnO core fiber is coated all-around with a continuous ZIF-8 shell layer in all the fibers (Fig. 8). Similarly to SEM it was evident in STEM that the treatment at 200 °C resulted in faster and more conformal conversion and thus more uniform fibers compared to the fibers subjected to the HmIM vapor at 150 °C. STEM showed that only a single phase could be identified in the fibers converted at 200 °C for 42 h, while the fibers converted at 150 °C for 18–68 h and at 200 °C for 18 h consisted of clear core and shell phases (Supporting information, Figs. S10 and S11). Thus the process enables the preparation of ZnO/ZIF-8 and AZO/ZIF-8 fibers with a distinct core/shell structure where the thickness of the core and shell can be controlled by the treatment time and temperature. The core/shell fibers could be interesting for gas sensing and energy storage applications [21].

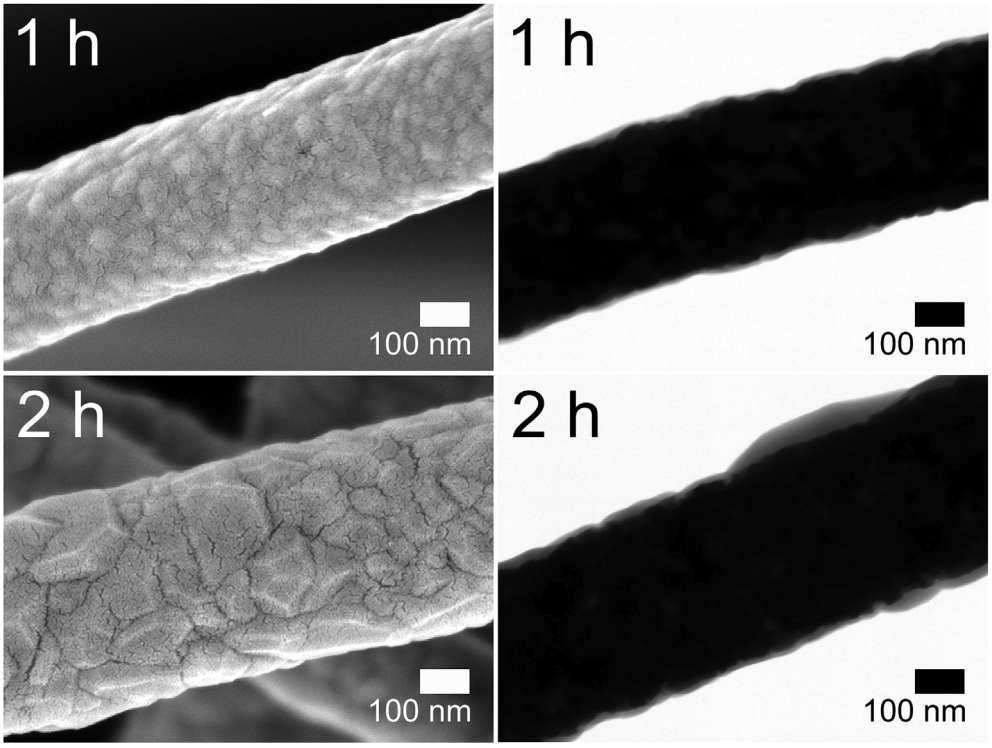

Fig. 7. High-magnification SEM and STEM images of ZnO fibers converted to ZIF-8 at 200 °C for 1 h and 2 h.

It is remarkable that the conversion can proceed so deep within the fiber core. Although the reaction seemed to be slowing down with increasing ZIF-8 layer thickness (Fig. 6), no limit for the reaction depth was found as the reaction seemed to continue until the whole fiber was converted. This suggests that probably even thicker fibers could be fully converted to ZIF-8 via this method and it should be similarly applicable to other ZnO structures, e.g. films and particles. In literature, gas phase conversion methods from ZnO to ZIF-8 have been employed to prepare thin films [8,9]. Stassen et al. demonstrated full and conformal conversion of sub 10 nm ZnO thin films [9]. In this study we could fully convert much thicker structures as the radii of the fibers that were converted were generally between 100 and 200 nm. This enabled the preparation of phase pure ZIF-8 fibers, though naturally in the fibers converted from AZO-3 also aluminum is present within the fibers in some form. It should also be noted that the gas phase conversion method used here can be expected to be applicable for the preparation of not only ZIF-8, but also other MOF fibers. Stassen et al. have demonstrated that gas phase conversion reactions can be used to prepare multiple different MOFs in thin film form [9]. Here we have shown that using a gas phase conversion in an autoclave fibers with diameters over 300 nm can be fully converted to ZIF-8. Electrospinning and electroblowing are capable of preparing a wide variety of oxide materials that could be used as templates for different MOF fibers using the gas phase conversion with appropriate ligands.

The textural parameters of the samples were determined from N_2 adsorption-desorption measurements. The specific surface areas of the fibers were determined by the Brunauer, Emmett and Teller (BET) method (Table 3). The isotherms showed a highly microporous structure for the samples. It can be seen that the specific surface area of the fibers was linearly increasing with increasing ZIF-8 content (Supporting information, Figs. S12 and S13). For the bare ZnO and AZO-3 fibers the BET surface areas were 5.28 and 31.2 m^2/g, respectively. The highest BET surface area of 1340 m^2/g was determined for the ZIF-8 fibers prepared by conversion of ZnO at 200 °C for 68 h. This result is comparable with BET surface areas generally reported in literature for particulate ZIF-8 prepared via various synthesis methods [67]. As compared to fibers converted from ZnO slightly smaller BET surface areas were obtained for the ZIF-8 fibers converted from AZO-3, most likely a consequence of the weight increasing aluminum dopant present within these fibers that results in a decrease in the surface area relative

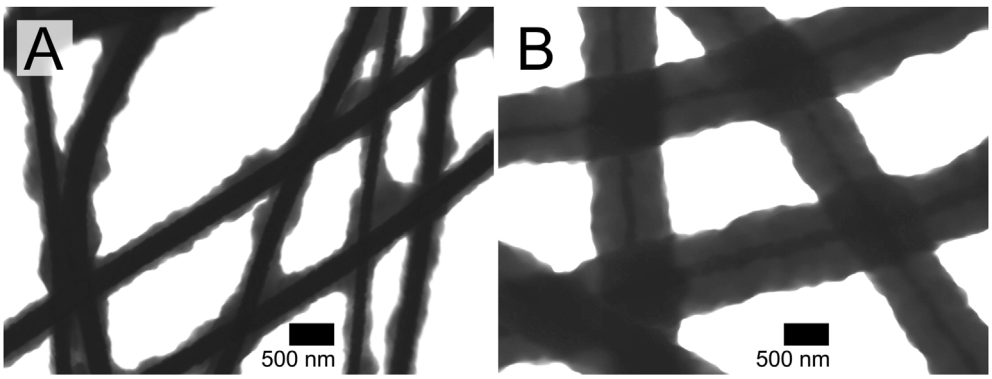

Fig. 8. STEM of ZnO/ZIF-8 core/shell fibers prepared by conversion of ZnO fibers under HmIM vapor at (A) 150 and (B) 200 °C for 18 h.

Table 3
BET surface area results of ZnO and AZO-3 fibers, and of fibers converted to ZIF-8 at 150 and 200 °C for 18–68 h.

Fibers	Conversion temperature	Conversion time	ZIF-8 content (wt. %)[a]	BET surface area (m^2/g)	t-Plot micropore area (m^2/g)	t-Plot external surface area (m^2/g)
ZnO	–	0 h	0	5.28 ± 0.01	0	5.47
ZnO to ZIF-8	150 °C	18 h	26	375 ± 8	368	7.7
		42 h	52	563 ± 13	549	14.4
		68 h	66	803 ± 17	769	33.4
	200 °C	18 h	88	1056 ± 22	1036	20.3
		42 h	99	1270 ± 26	1259	11.9
		68 h	100	1340 ± 28	1325	15.2
AZO-3	–	0 h	0	31.22 ± 0.04	2.1	29.1
AZO-3 to ZIF-8	200 °C	18 h	96	959 ± 20	939	20.1
		42 h	100	1225 ± 26	1206	18.6

[a] Determined using Rietveld refinement of the XRD data.

to the fiber weight. The measured pore size distributions showed the major micropore width to be 1.10 nm regardless whether ZnO or AZO-3 fibers were converted to ZIF-8 (Supporting information, Fig. S14). This result closely matches the theoretical ZIF-8 cage pore diameter of 1.16 nm [6].

4. Conclusion

ZnO and aluminum doped zinc oxide (AZO, 1–3 cation-% of Al) fibers were prepared for the first time by electroblowing. Electroblowing enabled the production of high quality continuous fibers at significantly improved rates compared to what has been previously reported. For the AZO fibers a production rate of 0.32 g/h was achieved. Higher Al content in the fibers led to a decrease in crystallinity. The prepared fibers could be converted to zeolitic imidazole framework-8 by thermal treatment under 2-methylimidazole vapor at 150 and 200 °C in an autoclave. Higher vapor conversion temperature resulted in faster conversion and more homogeneously converted fibers. Similarly lower initial crystallinity in the fibers promoted the conversion rate. The conversion progresses from the fiber surface towards the core of the fibers, thus enabling the conformal preparation of ZIF-8 fibers as well as also ZnO/ZIF-8 and AZO/ZIF-8 core/shell fibers depending on the conversion time. The process described here is not limited to thin ZnO layers as the fully converted ZnO fibers had originally diameters of 200–400 nm, i.e. the reaction could penetrate much deeper into the ZnO matrix than previously demonstrated in the literature. Similarly the conversion route enabled the preparation of bare ZIF-8 or any other MOF fibers for the first time, because the fibrous structure of ZnO could be retained through the full conversion due to the excellent conformality of the process. Owing to their microporosity the prepared ZIF-8 fibers had at best a very high specific surface area of 1340 m^2/g while in the bare ZnO fibers the area was only 5.28 m^2/g. The interconnected fibrous network structure combined with the high specific surface area makes the prepared fibers interesting especially for gas sensing applications but also a wide variety of electronic and optoelectronic applications. Also the conversion method in itself is applicable to not just fibers but to also other kinds of complex three-dimensional structures.

Acknowledgements

This work was supported by the Finnish Centre of Excellence in Atomic Layer Deposition.

Appendix A. Supplementary data

The following supplementary data related to this article is collected in a single pdf file: FESEM images of ZnO fibers with varying solvent combinations, XRD patterns of ZnO fibers calcined at different temperatures, A graph showing the effect of Al content on the resistance of AZO fiber sheets, Additional FESEM images of fibers subjected to the conversion treatment, XRD patterns of fibers converted to ZIF-8 at 200 °C for 18–68 h, TGA analyses of the ZIF-8 fibers, XRD studies on fibers converted for 1 and 2 h, STEM imaging of the converted fibers, N_2 adsorption-desorption measurements and pore size distribution studies on the fibers.

Supplementary data related to this article can be found at http://dx.doi.org/10.1016/j.micromeso.2018.04.003.

References

[1] J.Y. Lee, O.K. Farha, J. Roberts, K.A. Scheidt, S.B.T. Nguyen, J.T. Hupp, Chem. Soc. Rev. 38 (2009) 1450–1459.
[2] L.E. Kreno, K. Leong, O.K. Farha, M. Allendorf, R.P. Van Duyne, J.T. Hupp, Chem. Rev. 112 (2012) 1105–1125.
[3] V. Stavila, A.A. Talin, M.D. Allendorf, Chem. Soc. Rev. 43 (2014) 5994–6010.
[4] I. Stassen, D. De Vos, R. Ameloot, Chem. Eur J. 22 (2016) 14452–14460.
[5] Z. Li, J. Zhang, L. Yu, J. Zhang, J. Mater. Sci. 52 (2017) 6173–6195.
[6] K.S. Park, Z. Ni, A.P. Cote, J.Y. Choi, R. Huang, F.J. Uribe-Romo, H.K. Chae, M. O'Keeffe, O.M. Yaghi, Proc. Natl. Acad. Sci. U. S. A 103 (2006) 10186–10191.
[7] B. Chen, Z. Yang, Y. Zhu, Y. Xia, J. Mater. Chem. 2 (2014) 16811–16831.
[8] Y. Yue, Z. Qiao, X. Li, A.J. Binder, E. Formo, Z. Pan, C. Tian, Z. Bi, S. Dai, Cryst. Growth Des. 13 (2013) 1002–1005.
[9] I. Stassen, M. Styles, G. Grenci, H.V. Gorp, W. Vanderlinden, S.D. Feyter, P. Falcaro, D.D. Vos, P. Vereecken, R. Ameloot, Nat. Mater. 15 (2016) 304–310.
[10] N. Bhardwaj, S.C. Kundu, Biotechnol. Adv. 28 (2010) 325–347.
[11] S. Cavaliere, S. Subianto, I. Savych, D.J. Jones, J. Roziere, Energy Environ. Sci. 4 (2011) 4761–4785.
[12] Y. Dai, W. Liu, E. Formo, Y. Sun, Y. Xia, Polym. Adv. Technol. 22 (2011) 326–338.
[13] R. Ostermann, J. Cravillon, C. Weidmann, M. Wiebcke, B.M. Smarsly, Chem. Commun. 47 (2011) 442–444.
[14] M.R. Armstrong, B. Shan, S.V. Maringanti, W. Zheng, B. Mu, Ind. Eng. Chem. Res. 55 (2016) 9944–9951.
[15] M. Armstrong, C. Balzer, B. Shan, B. Mu, Langmuir 33 (2017) 9066–9072.
[16] M. Bechelany, M. Drobek, C. Vallicari, A. Abou Chaaya, A. Julbe, P. Miele, Nanoscale 7 (2015) 5794–5802.
[17] W. Zhang, Z. Wu, H. Jiang, S. Yu, J. Am. Chem. Soc. 136 (2014) 14385–14388.
[18] Z. Lian, L. Huimin, O. Zhaofei, Dalton Trans. 43 (2014) 6684–6688.
[19] M. Gao, L. Zeng, J. Nie, G. Ma, RSC Adv. 6 (2016) 7078–7085.
[20] X. Zeng, L. Huang, C. Wang, J. Wang, J. Li, X. Luo, ACS Appl. Mater. Interfaces 8 (2016) 20274–20282.
[21] M. Drobek, J. Kim, M. Bechelany, C. Vallicari, A. Julbe, S.S. Kim, ACS Appl. Mater. Interfaces 8 (2016) 8323–8328.
[22] X. He, C. Yang, D. Wang, S.E. Gilliland Iii, D. Chen, W. Wang, CrystEngComm 19 (2017) 2445–2450.
[23] V. Bhosle, J.T. Prater, F. Yang, D. Burk, S.R. Forrest, J. Narayan, J. Appl. Phys. 102 (2007) 023501.
[24] M. Gabás, E. Ochoa-Martínez, E. Navarrete-Astorga, A.R. Landa-Cánovas, P. Herrero, F. Agulló-Rueda, S. Palanco, J.J. Martínez-Serrano, J.R. Ramos-Barrado, Appl. Surf. Sci. 419 (2017) 595–602.
[25] X. Li, W. Ye, X. Zhou, F. Huang, D. Zhong, J. Phys. Chem. C 121 (2017) 10282–10288.
[26] J. Nomoto, Y. Nishi, T. Miyata, T. Minami, Thin Solid Films 534 (2013) 426–431.
[27] S.S. Mali, H. Kim, W.Y. Jang, H.S. Park, P.S. Patil, C.K. Hong, ACS Sustain. Chem. Eng. 1 (2013) 1207–1213.
[28] E. Ghafari, Y. Feng, Y. Liu, I. Ferguson, N. Lu, Composites Part B 116 (2017) 40–45.
[29] W. Wang, H. Huang, Z. Li, H. Zhang, Y. Wang, W. Zheng, C. Wang, J. Am. Ceram. Soc. 91 (2008) 3817–3819.
[30] W. Wu, J. Ting, P. Huang, Nanoscale Res. Lett. 4 (2009) 513.
[31] L. Liu, S. Li, J. Zhuang, L. Wang, J. Zhang, H. Li, Z. Liu, Y. Han, X. Jiang, P. Zhang, Sens. Actuators, B 155 (2011) 782–788.
[32] M. Zhao, X. Wang, L. Ning, J. Jia, X. Li, L. Cao, Sens. Actuators, B 156 (2011)

588–592.
[33] W. Li, S. Ma, G. Yang, Y. Mao, J. Luo, L. Cheng, D. Gengzang, X. Xu, S. Yan, Mater. Lett. 138 (2015) 188–191.
[34] S. Bai, S. Chen, Y. Zhao, T. Guo, R. Luo, D. Li, A. Chen, J. Mater. Chem. 2 (2014) 16697–16706.
[35] H.A. Khorami, M. Keyanpour-Rad, M.R. Vaezi, Appl. Surf. Sci. 257 (2011) 7988–7992.
[36] A. Katoch, J. Kim, Y.J. Kwon, H.W. Kim, S.S. Kim, ACS Appl. Mater. Interfaces 7 (2015) 11351–11358.
[37] B. Huang, C. Zhao, M. Zhang, Z. Zhang, E. Xie, J. Zhou, W. Han, Appl. Surf. Sci. 349 (2015) 615–621.
[38] Y. Zhao, X. Li, L. Dong, B. Yan, H. Shan, D. Li, X. Sun, Int. J. Hydrogen Energy 40 (2015) 14338–14344.
[39] X. Sun, Y. Huang, M. Zong, H. Wu, X. Ding, J. Mater. Sci. Mater. Electron. 27 (2016) 2682–2686.
[40] L. Qiao, X. Wang, L. Qiao, X. Sun, X. Li, Y. Zheng, D. He, Nanoscale 5 (2013) 3037–3042.
[41] D.Y. Lee, J. Cho, N. Cho, M. Lee, S. Lee, B. Kim, Thin Solid Films 517 (2008) 1262–1267.
[42] A.F. Lotus, Y.C. Kang, J.I. Walker, R.D. Ramsier, G.G. Chase, Mater. Sci. Eng. B 166 (2010) 61–66.
[43] D. Lin, W. Pan, H. Wu, J. Am. Ceram. Soc. 90 (2007) 71–76.
[44] D. Lin, H. Wu, W. Pan, Adv. Mater. 19 (2007) 3968–3972.
[45] Y. Cho, C. Kuo, J. Mater. Chem. C 4 (2016) 7649–7657.
[46] C.J. Luo, S.D. Stoyanov, E. Stride, E. Pelan, M. Edirisinghe, Chem. Soc. Rev. 41 (2012) 4708–4735.
[47] S.A. Theron, A.L. Yarin, E. Zussman, E. Kroll, Polymer 46 (2005) 2889–2899.
[48] D. Lukas, A. Sarkar, P. Pokorny, J. Appl. Phys. 103 (2008).
[49] H. Niu, X. Wang, T. Lin, J. Textil. Inst. 103 (2012) 787–794.
[50] O. Jirsak, F. Sanetrnik, D. Lukas, V. Kotek, L. Martinova, J. Chaloupek, Czech patent CZ294274B6, (2004) 13 pp.
[51] F. Zhou, R. Gong, I. Porat, Polym. Int. 58 (2009) 331–342.
[52] J. Holopainen, T. Penttinen, E. Santala, M. Ritala, Nanotechnology 26 (2015) 025301.
[53] E.S. Medeiros, G.M. Glenn, A.P. Klamczynski, W.J. Orts, L.H.C. Mattoso, J. Appl. Polym. Sci. 113 (2009) 2322–2330.
[54] P. Wojasiński Michal, Maciej, C. Tomasz, Pol. J. Chem. Technol. 16 (2014) 43.
[55] J.L. Daristotle, A.M. Behrens, A.D. Sandler, P. Kofinas, ACS Appl. Mater. Interfaces 8 (2016) 34951–34963.
[56] I.C. Um, D. Fang, B.S. Hsiao, A. Okamoto, B. Chu, Biomacromolecules 5 (2004) 1428–1436.
[57] M. Peng, Q. Sun, Q. Ma, P. Li, Microporous Mesoporous Mater. 115 (2008) 562–567.
[58] L. Li, W. Kang, X. Zhuang, J. Shi, Y. Zhao, B. Cheng, Mater. Lett. 160 (2015) 533–536.
[59] W. Tutak, S. Sarkar, S. Lin-Gibson, T.M. Farooque, G. Jyotsnendu, D. Wang, J. Kohn, D. Bolikal, C.G. Simon Jr., Biomaterials 34 (2013) 2389–2398.
[60] D. Tang, X. Zhuang, C. Zhang, B. Cheng, X. Li, J. Appl. Polym. Sci. 132 (2015) 42326.
[61] D.L. Costa, R.S. Leite, G.A. Neves, L.N.d.L. Santana, E.S. Medeiros, R.R. Menezes, Mater. Lett. 183 (2016) 109–113.
[62] S. Shi, X. Zhuang, B. Cheng, X. Wang, J. Mater. Chem. 1 (2013) 13779–13788.
[63] J. Holopainen, M. Ritala, J. Eur. Ceram. Soc. 36 (2016) 3219–3224.
[64] L. Lutterotti, D. Chateigner, S. Ferrari, J. Ricote, Thin Solid Films 450 (2004) 34–41.
[65] L. Lutterotti, Nucl. Instrum. Methods Phys. Res., Sect. B 268 (2010) 334–340.
[66] H.T. Kwon, H. Jeong, A.S. Lee, H.S. An, T. Lee, E. Jang, J.S. Lee, J. Choi, Chem. Commun. 52 (2016) 11669–11672.
[67] Y. Lee, M. Jang, H. Cho, H. Kwon, S. Kim, W. Ahn, Chem. Eng. J. 271 (2015) 276–280.